A frame and a hotspot in cochlear mechanics

C. Elliott Strimbu[1], Lauren A. Chiriboga[2], Brian L. Frost[3], Elika Fallah[2], Elizabeth S. Olson[1,2]

[1]Department of Otolaryngology, Head and Neck Surgery, Columbia University Vagelos College of Physicians and Surgeons, 630 West 168th Street, New York City, NY 10033

[2]Department of Biomedical Engineering, 1210 Amsterdam Avenue, Columbia University, New York City, NY 10025

[3]Department of Electrical Engineering, 1210 Amsterdam Avenue, Columbia University, New York City, NY 10025

abbreviated title: A frame and a hotspot in cochlear mechanics

corresponding author: Elizabeth S. Olson, eao2004@columbia.edu

The authors declare no financial interests or conflicts of interest.

Abstract:
Auditory sensation is based in nanoscale vibration of the sensory tissue of the cochlea, the organ of Corti complex (OCC). Motion within the OCC is now observable due to optical coherence tomography. In the cochlear base, in response to sound stimulation, the region that includes the electro-motile outer hair cells (OHC) was observed to move with larger amplitude than the surrounding regions. The intense motion is based in active cell mechanics, and the region was termed the "hotspot" (Cooper et al., 2018, Nature comm). In addition, motion within the central hotspot motion scaled nonlinearly with stimulus level at frequencies below the best frequency (BF), evincing sub-BF activity. Regions that do not exhibit sub-BF activity, which includes much of the OCC, are here termed the OCC "frame". The OCC frame is significant for auditory stimulation because hair cell stereocilia appear to lie within it. Thus, hair cell stimulation in the basal cochlea is shielded from sub-BF activity, except perhaps in pathological states. This report shows and discusses experimental data supporting the frame concept.

Significance Statement:
Auditory sensation is based in nanoscale vibration of the sensory tissue of the inner ear, the organ of Corti complex (OCC). Using optical coherence tomography, motion within the OCC was found to move differently than the OCC surface. This "hotspot" motion, which is due to active cell mechanics in the sensory hair cells, was relatively large but relatively less frequency resolved. The sensing stereocilia of the hair cells appear to lie within the OCC "frame," shielded from components of the hotspot motion that would be detrimental to frequency resolution, except perhaps in pathological states.

Introduction:

Phase-sensitive optical coherence tomography (OCT) has allowed observations of motion within the sensory tissue of the organ of Corti complex (OCC). Before OCT, observations were restricted to the first-encountered surface of the organ, which is the basilar membrane (BM) in the basal, high-frequency, region discussed in this report. Decades of observations revealed and confirmed that in healthy cochleae, frequency tuning at an auditory neuron was much like that of BM motion (Narayan et al., 1998). BM motion was nonlinear (it was elevated at low to moderate SPLs, and thus scaled compressively with sound level) likely due to active outer-hair-cell (OHC)-based forces driven by mechano-electric transduction (MET) current. The MET current saturates, leading to nonlinear OHC-based force (Fettiplace and Kim, 2014; Iwasa and Adachi, 1997). Thus, the non-linear motion is "active" motion. At the BM, activity was limited to the region of the best frequency (BF) peak, where *post-mortem* motion was reduced by factors approaching 1000 at low sound pressure levels (SPL). Sub-BF BM motion was unchanged *post-mortem*, and considered "passive" (Rhode, 2007). The OHC electro-mechanical transduction that is presumed responsible for the *in-vivo* activity is not tuned when measured in isolated OHCs (Frank et al., 1999) and the basis for the frequency tuning of nonlinear, active motion *in vivo* is not known, although creative cochlear models can predict this tuning (Nankali et al., 2020; Yoon et al., 2011).

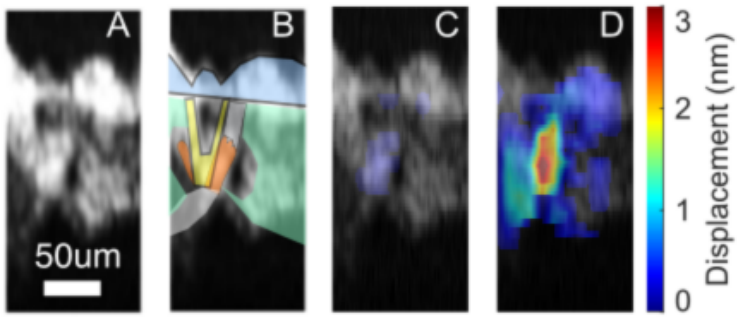

Figure 1. A. Brightness-scan (B-scan). The white regions are regions that reflect the OCT light, the dark regions are fluid spaces. B. B-scan with transparent cartoon of approximate anatomy with blue the BM, yellow the pillar cells, orange the outer and inner hair cells (OHC/IHC to the right/left of pillar cells). The white transparent regions below and above the OHCs are the tectorial membrane and Deiters cells respectively. (See Fig. 2A for detailed labelling of a radial-transverse cross section.) C-D. Motion response maps for 40 dB SPL multitone stimuli, at the frequencies BF/2 (C) and BF (D). Gerbil 995 run 23, BF ~ 31 kHz.

OCT-based measurements revealed motions in the OHC region of the sensory tissue that were greater than BM motion, leading to the term "hotspot" for the region (Cooper et al., 2018). The aptness of the term is clear in the motion maps in Fig. 1, from a healthy gerbil cochlea. Multitone stimuli were used and the responses mapped at the BF and half the BF. At both frequencies, motion is intense in the OHC region, referring to the anatomy roughly indicated in panel B. Motion within the hotspot also differed from the BM by showing active, nonlinear motion at sub-BF frequencies. Sub-BF nonlinearity appeared at relatively low SPL when multitone stimuli were used, likely because the simultaneous presence of near-BF tones led to saturation of MET current at low-moderate SPL. With single-tone stimuli sub-BF nonlinearity emerged at relatively high SPL (~ 80 dB SPL). The presence of sub-BF activity can also be perceived when sub-BF responses are reduced *post-mortem* (Strimbu et al., 2020; He et al., 2022; Cho and Puria, 2022). OHC-generated current is nonlinear (both at BF and sub-BF) at moderate SPL with multitone stimuli and is nonlinear at high SPL with single-tone stimuli, reaffirming the

expectation that nonlinearity in motion responses is due to MET current saturation (Fallah et al., 2019, Dong and Olson, 2013, 2016).

With this background we introduce the concept of the OCC "frame". The frame is defined as including all locations within the OCC that do not possess sub-BF activity. It is identified in this report as locations that do not exhibit nonlinear sub-BF motion in response to multitone stimuli. The results will show that the frame includes much of the OCC, including regions within the reticular lamina (RL), at the tectorial membrane-facing surface of the OHCs (Fig. 2A). With this observation, stereocilia are not stimulated by sub-BF activity. The opposite side of the OHCs, between the OHCs and Deiters cells, is termed the OHC\DC region. The discussion considers the measured OHC\DC-region motion as a sum of frame and internal-OHC\DC motion and reflects on the ramifications of the presence and absence of active sub-BF motion in different OCC regions.

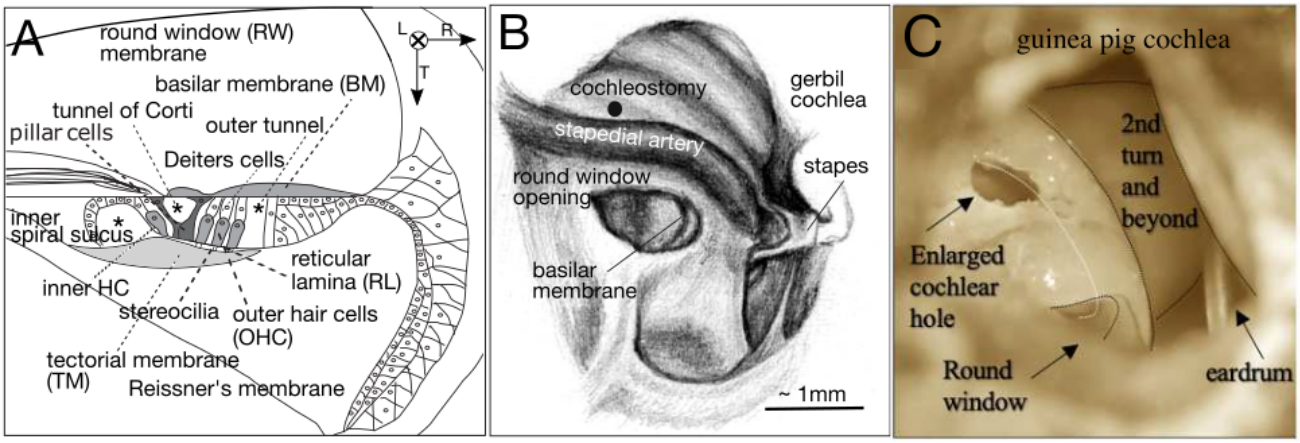

Figure 2. A. Cartoon of a cross section of the gerbil cochlear base; a transverse-radial B-scan gives this view. Radial, longitudinal and transverse directions are defined (L,R,T). The longitudinal direction points along the spiral of the cochlea, from the base towards the apex. Asterisks note the fluid tunnels that appear as dark areas and help parse the anatomy in a B-scan. B. Left gerbil cochlea. Motion measurements were made through the RW membrane, either with the optical axis transverse, in the very basal region, or with the optical axis pointing down the cochlear spiral to reach a lower BF region, with the optical axis including longitudinal and transverse components, and sometimes a significant radial component. The placement of a cochleostomy is shown. C. Surgical view of left guinea pig cochlea. A cochleostomy has been enlarged here for visualization. The white dotted line shows the path of the BM.

Methods:

The experiments were approved by the Institutional Animal Care and Use Committee of Columbia University. This report includes findings spanning several years of investigation in our lab, and several investigators, and longer versions of the methods can be found in Fallah et al., 2019 and Strimbu et al., 2020.

Animal preparation:

Juvenile guinea pigs of both sexes were used. Cochlear measurements were conducted while the animals were anesthetized with isoflurane inhalant. Buprenorphine was administered as an analgesic initially and after 6-8 hours. Some animals were also given subcutaneous injections of 2% lidocaine, ~.01. - .02 mL at each surgical site. The head of the animal was attached to a manipulator. A regulated heating blanket maintained the body temperature. The left bulla was opened with forceps using a posterior approach so that the round window (RW) and the first turn of the cochlea were

accessible (Fig. 2C). Measurements were made through the RW, and through a hole of diameter ~200-300 μm that was hand-drilled in the basal turn of the cochlear capsule, ~0.4 mm apical of the RW.

Adult gerbils of both sexes were used. They were initially anesthetized with intraperitoneal (IP) injections of 40 mg/kg ketamine and 40 mg/kg sodium pentobarbital. Buprenorphine, 0.1 mg/kg, was administered at the start of the surgery and after 6 – 8 hours. Supplemental doses of pentobarbital were administered to maintain areflexia in response to a toe pinch. Some animals were also given subcutaneous injections of 2% lidocaine. The animals were tracheotomized to facilitate breathing and their temperatures were maintained with a heating blanket. Supplemental heating was provided by a lamp and disposable hand warmers. The head was attached to a goniometer and the pinna and most of the cartilaginous ear canal (EC) and tissue covering the temporal bones were removed. The bulla was gently opened with forceps exposing the round window space. At the end of the experiment the animals, both guinea pig and gerbil, were euthanized with pentobarbital. Animal numbering is for internal record keeping.

Stimulation and response recording: Acoustic stimuli were generated by a Tucker Davis Technologies system and were presented closed-field to the EC by a Radio Shack dynamic speaker. A Sokolich ultrasonic microphone (WGS & Associates, Newport Beach, CA) was coupled to the speaker tube for sound calibration just inside the EC. Measurements at the ~ 25 kHz location in gerbils and guinea pigs were recorded at 98 kHz (97656.25 Hz) while those at higher frequency locations were recorded at 130 kHz (130208.33 Hz). The multitone stimuli used here were zwuis tone complexes in which *N* frequencies are played simultaneously (van der Heijden and Joris, 2003). The frequencies were chosen to have an integer number of cycles in the recording window, approximately equal spacing (up to a few percent), and had no harmonics or intermodulation distortion products up to third order. Each sinusoidal component of the complex was assigned a random phase so the total sound pressure level, in dB SPL, was ~ 10 log *N* higher than each individual frequency component. Single-tone stimuli were presented as discreet sweeps in which each frequency was presented for 63 ms including a 1 ms rise/fall tapered with a cosine-squared envelope. Single-tone stimuli were played with a higher maximal level to cover the same dynamic range as the multitone stimuli. Recordings were 1 s in length except for the data in Fig. 10 and Fig. 11, which were 10 s and 5 s respectively.

OCT: Displacement measurements were acquired using a Thorlabs Telesto 311 spectral domain OCT system with a central wavelength of 1300 nm. OCT produces a 1-D "image" within the depth of the preparation, which is termed an axial scan (A-scan); scanning with mirrors along a second axis produces a 2-D image termed a B-scan. The ThorImage program was used to generate B-scans to orient the preparation and locate the regions of interest within the cochlea, and for volumetric (3-D) imaging. The OCT system is equipped with an LSM03 objective lens, and the properties of the light source and lens determine the system's imaging resolution. The system has an axial resolution of approximately 8.3 μm and a lateral resolution of approximately 8 μm. The vertical positions of measurement locations in a B-scan are noted in pixels, and the distance between adjacent pixels is 2.7 μm. A time series of A-scans (M-

scans) was taken at selected regions in the cochlea, to measure vibration. Acquisition and initial processing of the OCT vibrometry data were performed using custom software written in C++ using the Thorlabs Spectral Radar software development kit.

Experimental design:

Measurements made with an M-scan along a single axis were typically made close to the intersection of the arcuate and pectinate zones, passing through the outer hair cell region. Area-spanning recordings of the uniaxial vibrations, which can be represented as heat maps as in Fig. 1, were constructed by taking sequential M-scans in 10 μm radial steps. To confirm that the structures were stable over the length of the recordings, the OCT software took structural B-scans of the same region before and after each set of vibration measurements and we compared the two images to exclude recordings with significant drift. Further offline analysis was performed in custom software written in MATLAB. Once the vibration time waveforms were acquired for the regions of interest, the amplitudes and phases at the sound stimulus frequencies were extracted by Fourier analysis. For each stimulus frequency, the response was deemed significant if the Fourier coefficient was 3 times larger than the standard deviation of the noise level, measured from 10 neighboring bins in the spectra.

The report here includes OCT-observations made over several years in several studies. However none of the specific data here were previously published. A common aspect of experimental design in these studies was to simultaneously observe and compare motion at different locations within the sensory tissue of the OCC. The studies sometimes pursued specific hypotheses, for example regarding the effect of ototoxic drugs (Strimbu et al. 2020, 2022), but the results here are of unperturbed cochleae.

Analytical methods:

Longitudinal, radial, transverse components of the optical axis: Frost et al., 2022 outlined a program in which a volume scan is used to generate the mapping between anatomical coordinates (the longitudinal (L), radial (R), transverse (T) directions noted in Fig. 2A) and optical coordinates from an OCT volume scan. For some of the data sets here L, R, T components of the optical axis are reported. The relative values of these components indicate how much each of these directions is represented in the measured motion. For example, in Fig. 3, the relative L, R, T components were 0.85,0.24,0.47, signifying that the optical axis was primarily in the longitudinal direction but with substantial transverse and radial contributions. Motion along any of the anatomical axes would contribute to the displacement measurement, with the actual motion in each anatomical direction weighted by its respective signed component in the reported motion.

Complex differences: The complex difference of two quantities, $G=G_o e^{(i\phi_G)}$ and $F= F_o e^{(i\phi_F)}$ can be done automatically with MATLAB, which works seamlessly with complex quantities. Alternatively, the polar forms (magnitude and phase) of G and F can be first written in rectangular form as $G=G_o(\cos(\phi_G) + i\sin(\phi_G))$, and similarly for F. The difference, D, is found as $D_{real}=G_{real} - F_{real}$, $D_{imag}=G_{imag} - F_{imag}$. Finally, D is converted to polar form as $D_o=[D_{real}^2 + D_{imag}^2]^{1/2}$ and $\phi_D=\arctan(D_{imag}/D_{real})$.

Results

A. Comparison of multitone and single-tone responses

Fig. 3 illustrates the multitone versus single-tone difference in motion responses in the gerbil cochlea (Fallah et al., 2019; Versteegh et al., 2012). It shows frequency response gains at the BM (upper

panels) and the OHC\DC region (lower panels) with single-tone (A) and multitone (B) stimuli. In Fig. 3C a subset of the single-tone data are plotted as dashed lines along with multitone data.

Responses are shown to stimuli spanning 45 to 95 dB SPL in the single tone measurements, and 40 to 80 dB SPL in the multitone measurements. If the responses scaled linearly, within a single panel all the curves would overlie. Thus, at least within the BF peak all these responses are compressively nonlinear, meaning that the higher SPL gains are below the lower SPL gains. At low SPL all the responses peaked at ~ 30 kHz, the BF.

At the BM, for both single and multitone stimuli, all gains were equal at frequencies below 20 kHz. The responses are passive; they are as they would be without activity. The 95 dB SPL single-tone gains and 80 dB SPL multitone gains were identical through the full frequency range, including the BF (Fig. 2C, upper). These responses can also be considered passive; in this case the passive responses to sound have dominated active contributions, which have saturated at a level that makes them insignificant.

In the OHC\DC-region, the single-tone responses scaled linearly up to 75 dB SPL at frequencies up to 15 kHz, whereas the multitone responses already showed nonlinear scaling at 40 dB SPL. In the OHC\DC-region comparison in Fig. 3C (lower panel), at frequencies up to 15 kHz the multitone gain at 60 dB was comparable to the single-tone gain at 95 dB, and the multitone gain at 53 dB was comparable to the single-tone gain at 85 dB. Above 15 kHz and through the peak region, the multitone gain at 80 dB was comparable to the single-tone gain at 95 dB.

In the BM data (upper panels, Fig. 3A&B) the highest SPL data from the OHC\DC region are included as dotted lines to make an OHC vs BM comparison. With the multitone data (B), sub-BF, the 80 dB SPL responses from the OHC\DC region were similar to responses in the BM region. Contrast this with the single-tone responses (A), where even at 95 dB SPL the sub-BF OHC\DC region responses were larger than the BM responses, meaning OHC activity remained significant. A point of these observations is that multitone stimuli are better able to identify nonlinearity (activity) in the sub-BF region than single-tone stimuli (barring the experiment-ending step of *post-mortem* measurements, in which case either stimulus type will serve). Multitone stimuli were used in what follows.

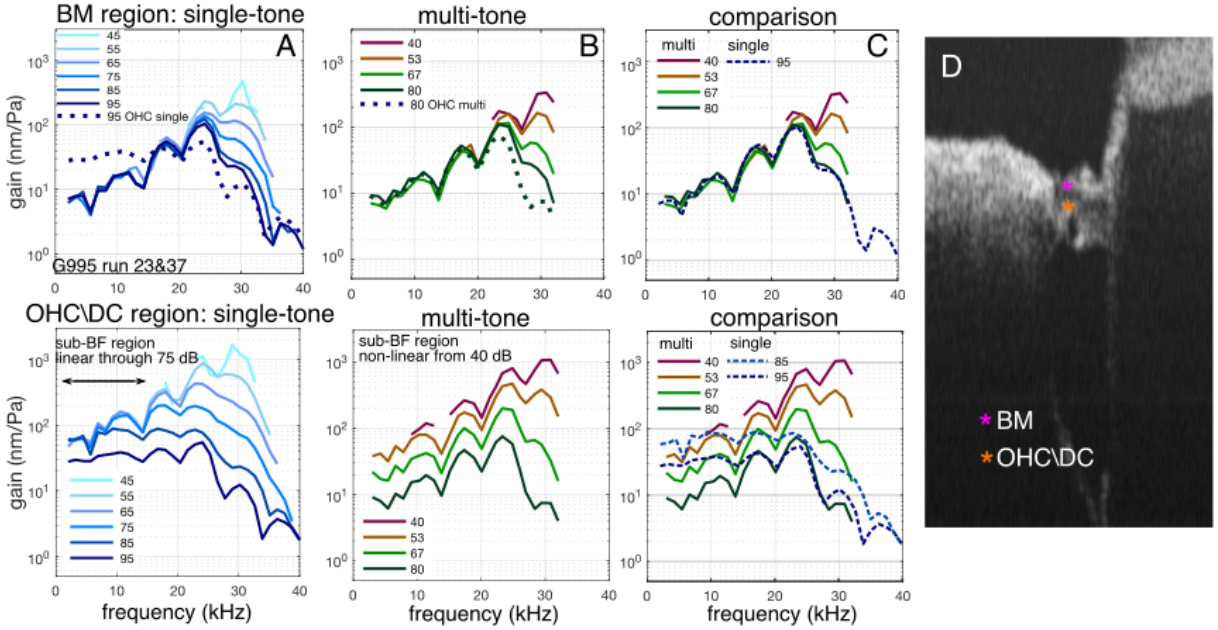

Figure 3. A-C. Comparison of multitone (A) and single-tone (B) responses, with direct comparisons in (C). D. B-scan showing locations of displayed motion responses. Responses are normalized to EC pressure as gains, so nonlinearity is apparent

when curves at different stimulation levels do not overlap. Data were taken through the gerbil RW, with the optical axis aimed apically to reach the ~ 30 kHz BF location. The optical axis had significant components in all three anatomical axes, with longitudinal, radial and transverse components of 0.85, 0.24, 0.47 (see methods for explanation). Gerbil 995 runs 23&37.

B. Examples to illustrate the concept of the frame.

The remainder of this section consists of examples of motion measurements, chosen to illustrate the concept of the frame. Except for Fig. 3, all the data shown were taken with multitone stimuli. The presence of sub-BF nonlinearity was evaluated at frequencies less than BF/2, by evaluating the overlap of the gain curves. Motion observed in several different locations is reported: (1) Gerbil ~ 45-50 kHz BF place, taken through the RW with a view that is approximately transverse. (2) Gerbil ~ 24 kHz BF place. These measurements were typically made by viewing apically down the cochlea from the round window (RW), with the viewing axis containing substantial components in the longitudinal and transverse directions and sometimes also the radial direction (the anatomical directions defined in Fig. 2A as L, R, T). One data set is included that was taken through a cochleostomy in gerbil, affording a nearly transverse view at the ~ 24 kHz place. (3) Observations from guinea pig that reinforce findings from gerbil. The views in guinea pig had little or no longitudinal component and were taken either through the RW, ~ 40 kHz place or through a basal cochleostomy, ~ 25 kHz place (Fallah et al., 2021).

1. Gerbil - optical axis in approximately transverse direction

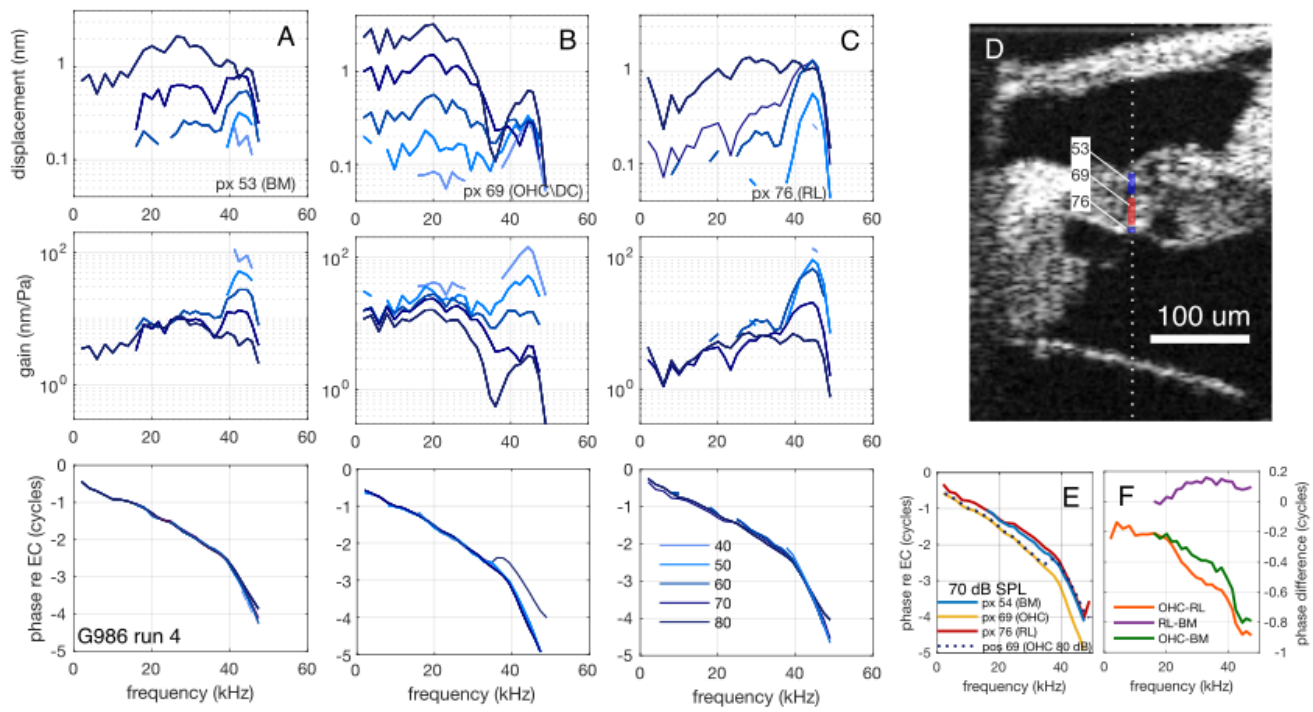

Figure 4. Results taken with an essentially transverse optical axis, and illustrating the concept of non-frame and frame. A-C. Results from three positions along one axial scan (A-scan). The top panels are displacement, middle are gain (displacement/EC pressure) and bottom are phase relative to EC pressure. A,B, and C each represent one of the regions indicated in the three transparent vertical bars overlying the A-scan (dotted line) in the B-scan of (D). The two blue bars include positions identified as being in the frame (those lacking sub-BF nonlinearity), the red bar includes points that contained sub-BF nonlinearity. Anatomically, pixels 53, 69 and 76 are within the BM, OHC\DC-region and RL-region respectively. Panels E and F compare phases measured at 70 dB SPL. Gerbil986 run4.

Fig. 4 shows three motion data sets (A-C) and the associated B-scan (D). Based on the analysis described in the methods, the optical axis was essentially transverse. The measurements were made through the RW opening, along one A-scan, the dotted line in D. The positions of the measurements in panels A, B and C spanned 23 pixels, corresponding to 62 μm. Anatomically, pixels 53, 69 and 76 were within the BM, OHC\DC-region and RL-region, respectively. The BF was ~ 42 kHz. The sub-BF responses at pixel 69 (OHC\DC, Fig. 4B) were elevated relative to those at pixels 53 (BM) and 76 (RL), and sub-BF nonlinearity was evident. Thus pixel 69 (OHC\DC) is not in the frame. Pixels 53 (BM) and 76 (RL) (Fig. 4 A&C) did not exhibit sub-BF nonlinearity below 21 kHz and are in the frame. Positions that were in the frame are within the two blue vertical bars that overlie the white dotted A-scan line**.** Positions that were not in the frame (contained sub-BF nonlinearity) are within the red vertical bar that overlies the A-scan line. Some oddities of the data are the amplitude trough at high SPL in the OHC\DC region (Fig. 4B upper and middle panels), occurring along with a phase shift (Fig. 4B lower panel). (The word "trough" is used rather than "notch" because the reduction can span a relatively wide range of frequency.) The interpretation of this behavior benefits from a complex-difference analysis, performed in the first part of the discussion. Fig. 4E shows the phases from the three positions at 70 dB SPL and phase differences are shown in Fig. 4F. 70 dB SPL data are shown because there was not much variation between SPLs except at 80 dB SPL and the 70 dB SPL data are out of the noise through a relatively wide frequency range. In Fig. 4E, 80 dB SPL OHC\DC region phase is included and shows that at frequencies above the phase shift, the OHC\DC phase was in line with the BM and RL phases. The RL phase led the BM phase by a value that increased from ~ 0 to ~ 0.15 cycle from 18 to 35 kHz. The possible significance of this lead is noted in the final section of the discussion. The OHC\DC region was close to half a cycle out of phase with the RL (varying between 0.4 and 0.6 cycles difference) from 20 to 40 kHz.

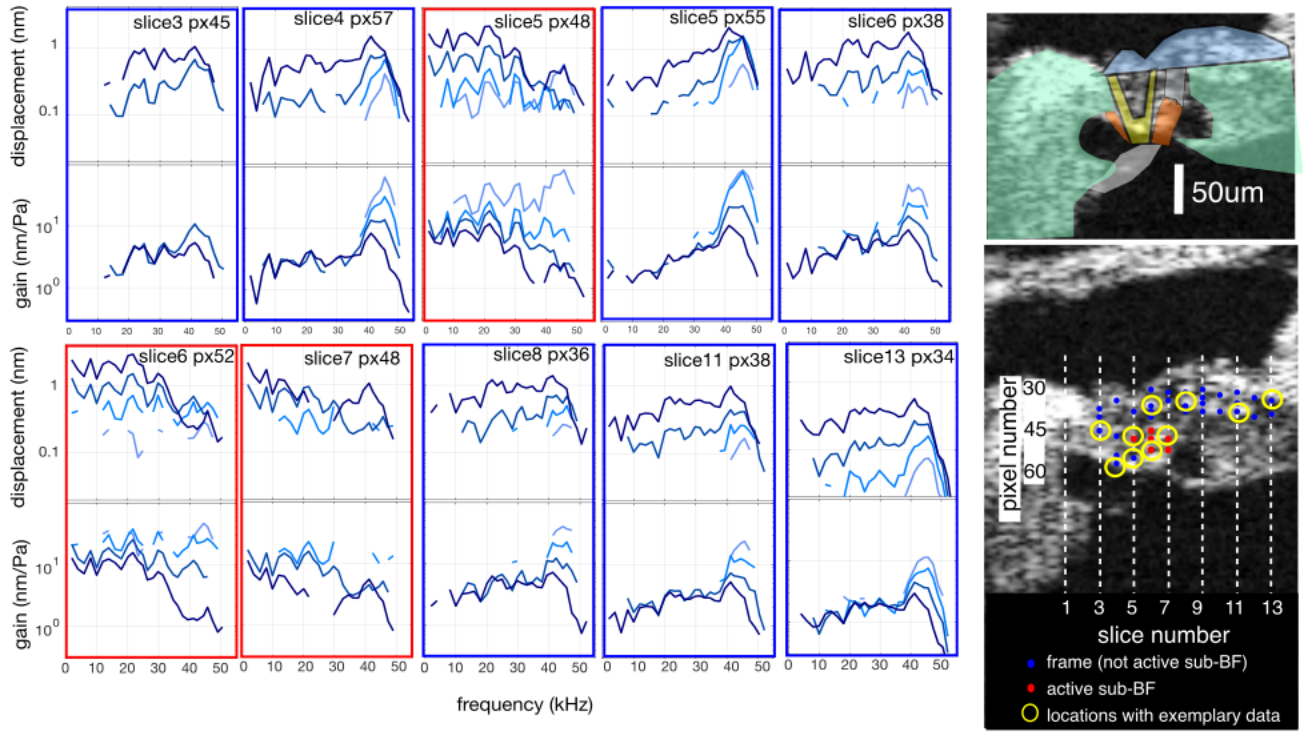

Figure 5. Frame map. A series of A-scan "slices" generated a set of motion observations, indicated in the dots in the orienting B-scan at the bottom right. Above the orienting B-scan is a cartoon of approximate anatomy with coloring as in Fig. 1B. The optical axis had relative longitudinal, radial and transverse contributions of 0, .02, 0.99 respectively, so was nearly transverse. The blue/red dots indicate frame/not-frame. The yellow circles identify locations where exemplary data are shown in the

panels at the left, with the blue/red boxes corresponding to the locations with blue/red dots. Multitone stimuli were applied at 50, 60, 70, 80 dB SPL (lighter to darker blue). Each data set is shown both as displacement and as gain; the gain curves make it easier to identify sub-BF nonlinearity and the displacement curves expose data that can be covered by other data in the gain curves. Gerbil986 run 11.

The measurements shown in Fig. 5 were made through the RW after those of Fig. 4, following slight repositioning. The optical axis was transverse. The BF was ~ 45 kHz. At the right of Fig. 5 is a B-scan, showing A-scan locations where motion was measured. At every point in which the data were sufficient to evaluate sub-BF linearity a red or blue dot is shown, indicating presence (red) or absence (blue) of sub-BF nonlinearity. "Sub-BF" evaluation refers to frequencies below 23 kHz (~ BF/2). A subset of displacement and gain responses is shown in the plots to the left, and their locations indicated by the yellow circles. Three exemplary data sets are shown from the sets that possessed sub-BF nonlinearity (red points). They contained an amplitude trough at 80 dB SPL (most obvious in the gain curves), like in Fig. 4B. The other exemplary data sets are from the blue, frame points. A purpose of this figure is to demonstrate the "frame-like" characteristics of many points -- to show the lack of sub-BF nonlinearity and amplitude troughs outside the OHC\DC region. In the lateral region to the right of slice 7, the blue dots are all within what is likely the BM. The deeper lateral region lacks points because waning reflectivity led to noise levels close to 1 nm, making evaluation of sub-BF scaling impossible. A frame map in Fig. 9 includes frame points within the lateral region.

Fig. 6 is another measurement made through the RW in gerbil with the optical axis nearly transverse, with slightly higher BF, ~ 52 kHz. It reinforces observations of Fig. 4 and 5: sub-BF linearity in the BM and RL regions (A and C), and sub-BF nonlinearity in the OHC\DC region (B) along with an amplitude trough and phase shift at high level (80 dB SPL). The phase differences shown in Fig. 6 E&F are similar to those of Fig. 4, with nearly half cycle difference between the OHC\DC region and the RL from 30 to 50 kHz, the RL leading the BM by up to 0.2 cycles, and the 80 dB OHC\DC-region phase lifting to join the BM and RL phase at frequencies above those of the trough.

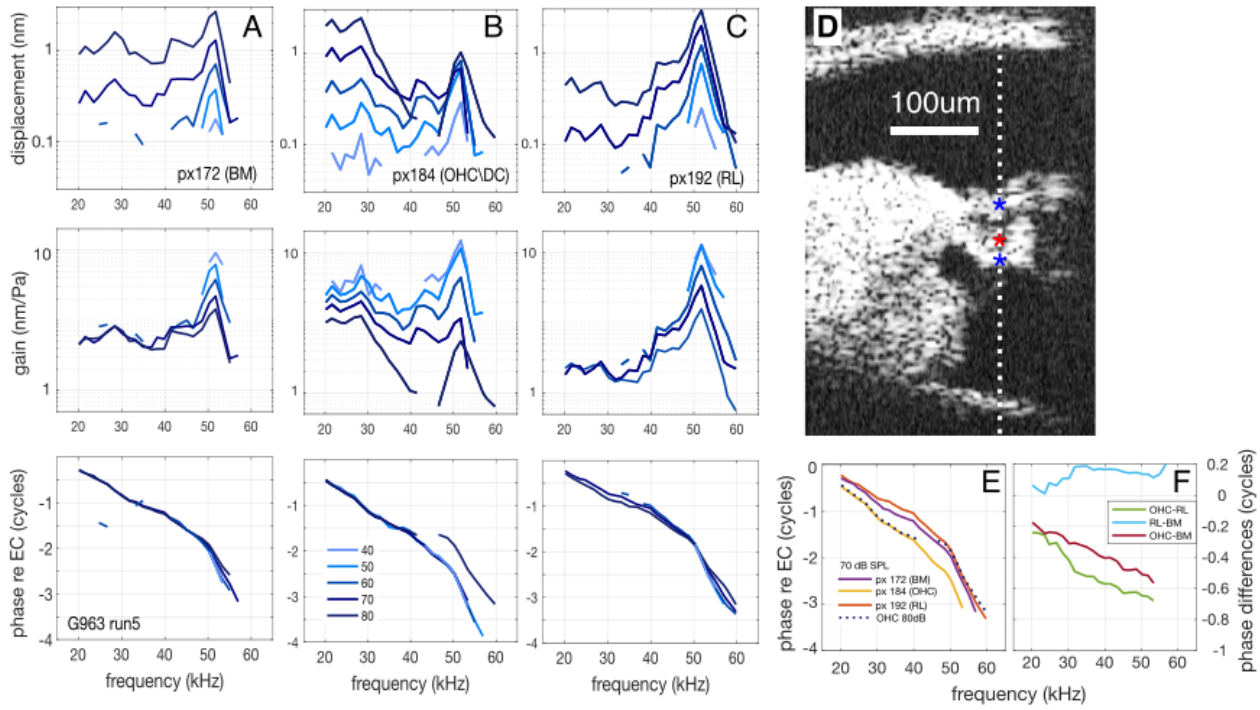

Fig. 6. Another example of transverse data, with a similar lay-out as Fig. 4. In D, the asterisks indicate the positions of the recordings in A-C, and the pixel values are noted. Red/blue asterisks indicate non-frame/frame. Gerbil 963 run 5.

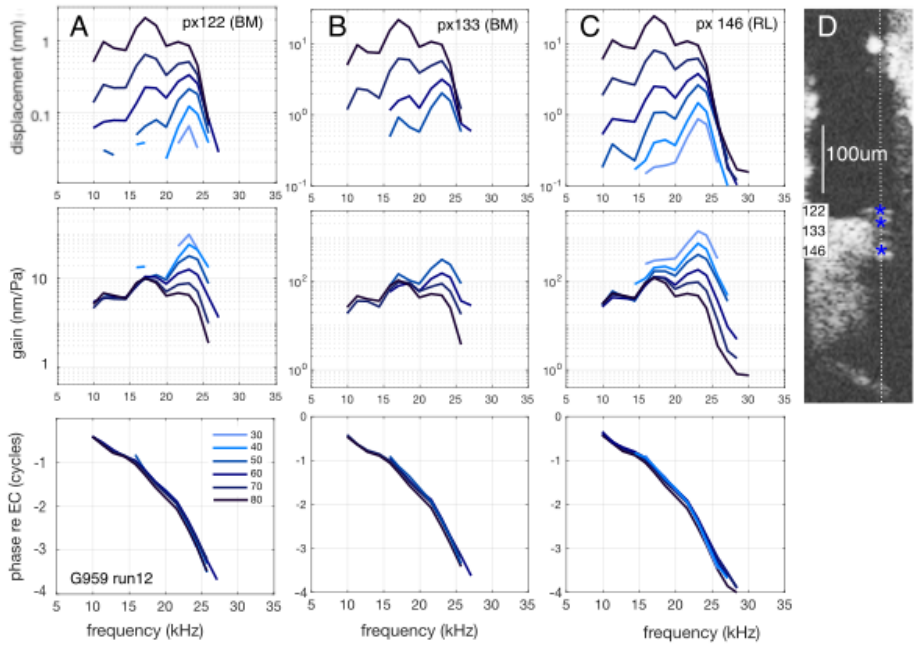

Figure 7. Data taken through a cochleostomy as in Fig.2B. Viewing axis was nearly transverse. Only the very medial region of the OCC was visible. Results from three positions along one A-scan are shown in (A), (B) and (C) indicated in the asterisks and with their pixel values in the B-scan of (D). All these data are within the frame, without sub-BF nonlinearity. Gerbil 959 run 12.

In Figs. 7 and 8 we show two data sets from the ~ 23 kHz BF location from the same gerbil. Fig. 7 data were taken through a cochleostomy made above the stapedial artery (Fig. 2B), affording a nearly transverse view but limited to the very medial region of the OCC. The Fig. 7 results did not include any locations with sub-BF nonlinearity; thus the three positions are within the OCC frame. Points A and B are close to or within the BM, point C, 65 μm deeper than point A, is within or close to the RL. The phases were similar across these locations.

2. Gerbil - optical axis containing substantial longitudinal component.

Fig. 8 data were from the same gerbil as Fig. 7, taken through the RW with the optical axis pointing apically to reach nearly the same BF location, and thus with a substantial longitudinal component. The BM responses in Fig. 8A were qualitatively similar to the BM responses in Fig. 7, with a direct comparison of 60 dB data included in Fig. 8A (green dashed lines in the middle and lower panels). The BM is expected to move purely transversely, which would reduce the magnitude of the measured BM motion in Fig. 8 compared to Fig. 7 by a value of the relative transverse component of the optical axis. For example, if that value was 0.5 and these measurements were made at the same radial location across the width of the BM, we would expect the green line to lie at twice the value of the Fig. 8 line. However, the Fig. 7 data were collected medial, closer to a rigid boundary, at a position that would move less than a more central radial position. Thus, there are two competing effects, and the result, with the green line from Fig. 7 a little above the Fig. 8 lines, lies at a reasonable level. The Fig. 7 data peak at a just slightly higher BF, due to inexact matching of BF location, but the overall similarity in the Fig. 7 and Fig. 8 data support the view that the BM moves transversely, with motion that is similar, simply scaled, at different radial locations and viewing angles (Frost et al., 2022; Cooper et al., 2018).

The B-scan in Fig. 8D is distorted from the transverse-radial view (Fig. 2A) due to the non-transverse optical axis, and the most obvious landmarks are the dark regions that correspond to the outer tunnel (below red bar) and tunnel of Corti (above-left of red bar), which sandwich the OHC\DC region. The motion at the BM (Fig. 8A) and ~120 μm within the OCC, in the cells that are lateral to the outer tunnel (Fig. 8C) scale linearly sub-BF, and are in the OCC frame. The OHC\DC-region motion (Fig. 8B) showed sub-BF nonlinearity. The OHC\DC region also showed an amplitude notch and phase shift at the highest SPL, but the phase shift is different from that in Figs. 4 and 6; in Figs. 4 and 6 the OHC phase shifted to join the BM phase, in Fig. 8 the OHC\DC-region phase was generally similar to BM phase (dotted pink line gives a direct comparison) and the notch-related phase shift at 80 dB shifted the phase away from the BM phase. The amplitude notch and phase shift here are likely related to the OHC\DC-region motion being nearly perpendicular to the viewing axis when the viewing axis is substantially longitudinal (Frost et al., 2022, 2023a, 2023b). At frequencies below 15 kHz the OHC\DC region led the BM slightly (pink dotted line) as in results from our previous reports with this optical approach (Strimbu et al., 2020).

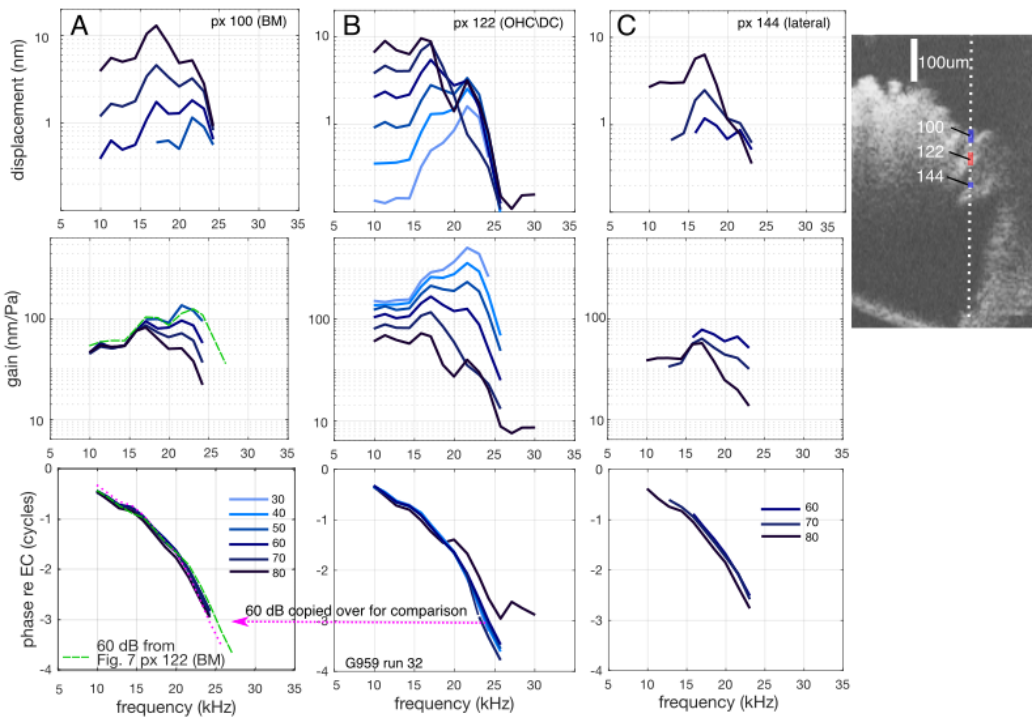

Figure 8. Responses at the same BF location as Fig. 7, with data here taken through the RW opening, with a substantial longitudinal component to the optical axis. A-C. Results from three positions along one A-scan. Each represents one of the regions indicated in the three vertical lines along the A-scan noted as a dotted line in the B-scan of (D). The blue vertical bars in (D) include points in the frame (those lacking sub-BF nonlinearity), the red vertical bar includes points that contained sub-BF nonlinearity. Anatomically, pixels 100, 122 and 144 are within the BM, OHC\DC region and lateral region respectively. In the BM panels (A), two comparisons are included. The pink dotted line is the phase responses from the OHC\DC region. The green dashed lines are the gain and phase responses copied from the BM pixel 122 in Fig. 7. Gerbil 959 run 32.

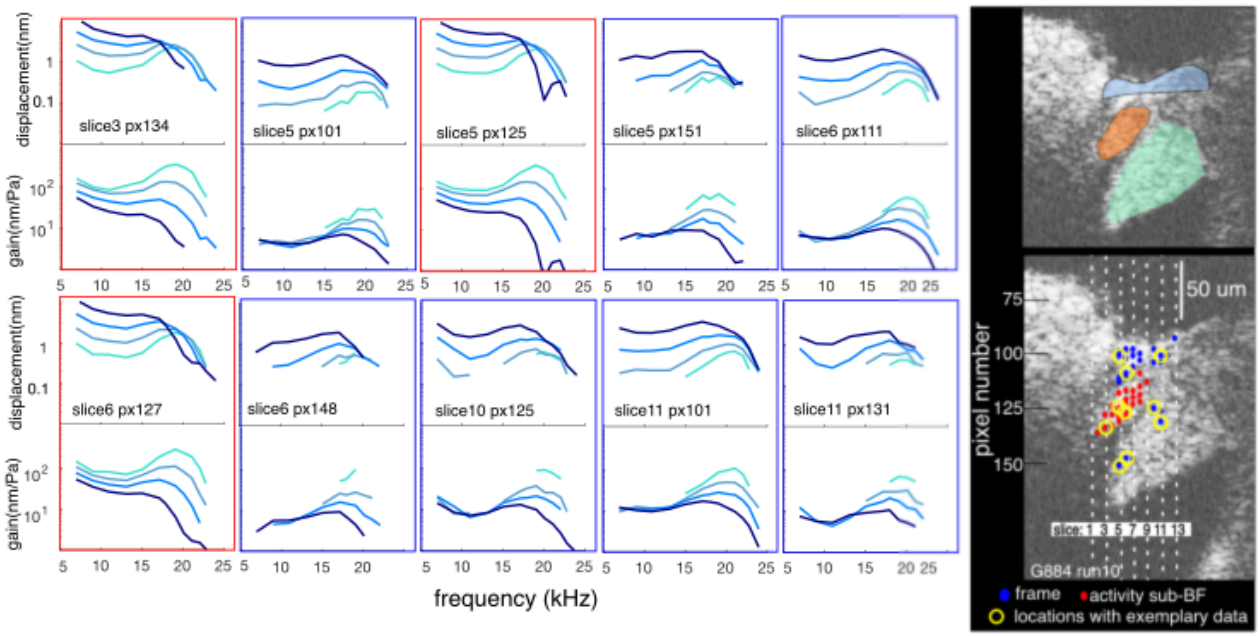

Figure 9. Frame map. Similar layout as Fig. 5. Multitone stimuli were applied at 50, 60, 70, 80 dB SPL (lighter to darker blue). Due to the longitudinal view, the B-scan was not a radial-transverse view. Rough color-coding in the upper B-scan with the transparent anatomical map is based on the dark areas of the outer tunnel and tunnel of Corti. Blue is basilar membrane, orange is OHC region, green is lateral region. Gerbil 884 run 10.

The measurements in the frame map of Fig. 9 were made with the optical axis primarily longitudinal to reach the ~ 20 kHz BF location. Displacement data are shown in the plots to the left of the orienting B-scan. As in Fig. 8, the dark fluid-filled spaces above and below the OHC\DC region were useful in identifying that region. Three exemplary data sets are included from the sets that possessed sub-BF nonlinearity (red points). These points also show notches and hyper-compression, in which displacement at higher SPL lies below displacement at lower SPL. The other exemplary data sets are from blue, frame points. The BM and lateral region were within the frame, and the area showing sub-BF nonlinearity was within the OHC\DC region, which was elongated due to the longitudinal view. Fig. 10 is a final example taken with a substantial longitudinal optical axis. Results from two A-scans are shown, the left A-scan goes through the OHC\DC region, the right A-scan is lateral. Of the seven measured locations, only the location within the OHC\DC region (B) exhibited sub-BF nonlinearity. Location A, D and E were within the BM, and location F and G were within the lateral region. Location C looks to be within the RL. It was often not possible to visualize and thus probe the RL with the longitudinal approach. We include this data set to support the results from the more transverse view (Figs. 4-7) in which the RL does not present sub-BF nonlinearity and thus was within the OCC frame.

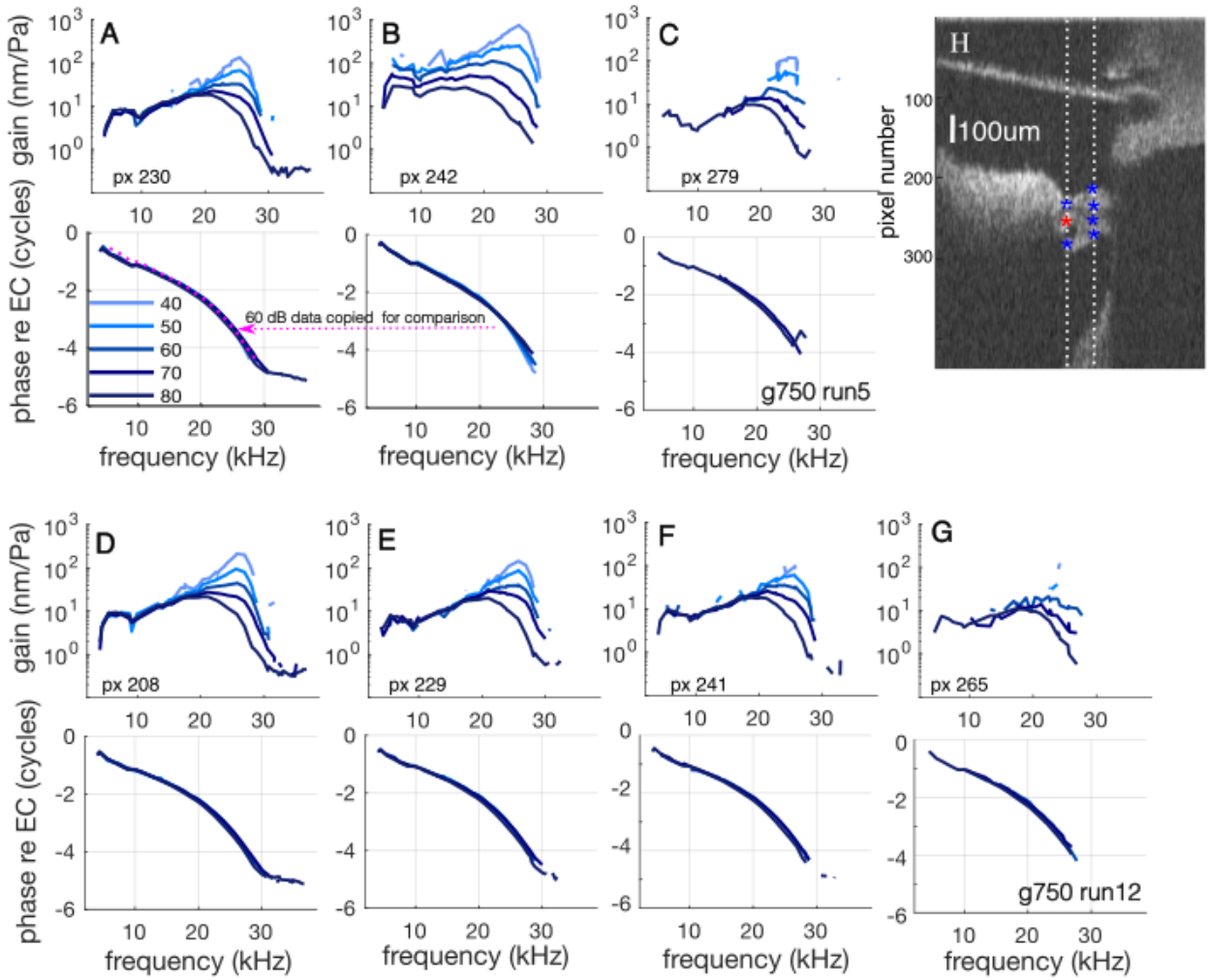

Figure 10 -- Another example in which data were taken through the RW opening, with a substantial longitudinal component to the optical axis. Responses were measured over two A-scans, indicated in the asterisks in the B-scan in H. A-C are from the left A-scan, D-G are from the right A-scan. The blue/red asterisks indicate frame/not-frame (absence/presence of sub-BF nonlinearity). Multitone stimuli were applied at 40, 50, 60, 70, 80 dB SPL (lighter to darker colors). Gerbil 750, runs5&12.

3. Guinea Pig - observations with optical axis lacking longitudinal component.

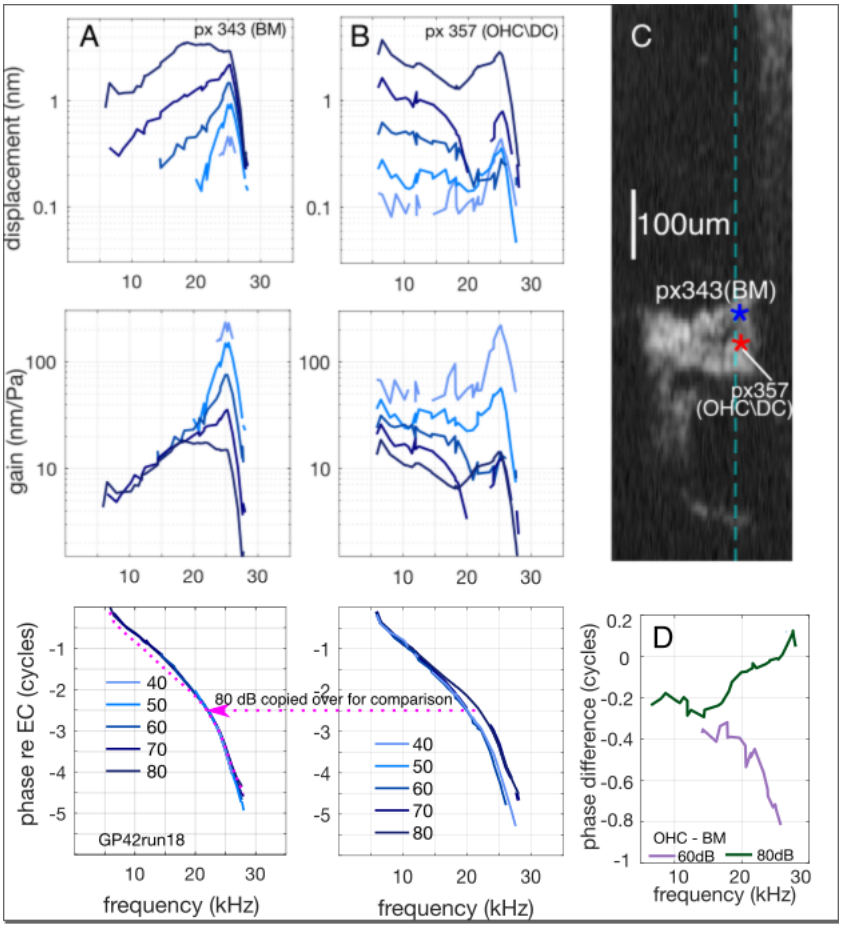

Figure 11. Measurements in a guinea pig show similarities to gerbil data. (A-B) These measurements, made through a cochleostomy as in Fig. 2C, were nearly transverse. C. Responses were measured at the locations indicated in the asterisks in the B-scan. Multitone stimuli were applied at 40, 50, 60, 70, 80 dB SPL (lighter to darker colors). The blue/red asterisks indicate frame/not-frame and correspond anatomically to BM/OHC-region. The reflectivity of deeper regions was insufficient to measure motion within the RL. D. Phase differences at 60 and 80 dB SPL. Guinea pig 42 run18.

The guinea pig results in Fig. 11 were measured through a cochleostomy to access the ~ 25 kHz BF place with an approximately transverse optical axis. Strong sub-BF nonlinearity was observed in the OHC\DC region (Fig. 11B). The Fig. 11 results show similarities to the transversely measured gerbil data of Figs. 4-6, namely, the OHC-region location contained sub-BF nonlinearity, and an amplitude trough at high SPL (70 and 80 dB SPL). The phase in the OHC\DC region was close to half-cycle out of phase with the BM phase from ~ 15-24 kHz (60 dB curve in (D)) except at high SPL (80 dB curve in (D)), where the phase shifted to meet the BM phase.

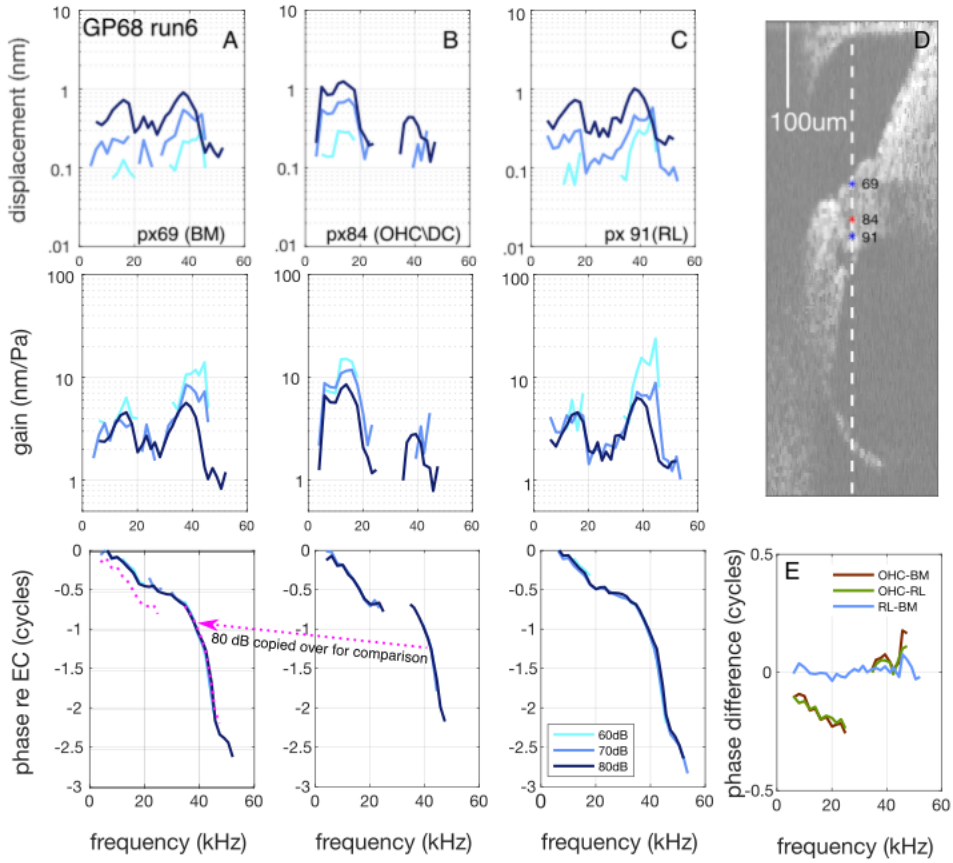

Figure 12 Measurements in a guinea pig through the RW. (A-C) In these data the optical axis contained significant transverse and radial components, but little to no longitudinal component. Responses were measured at the locations indicated in the asterisks in the B-scan to the right (D). Multitone stimuli were applied at 60, 70 and 80 dB SPL (lighter to darker colors). The blue/red asterisks indicate frame/not-frame and correspond anatomically to BM, OHC-region and RL region. The phase data from the OHC\DC region 80 dB response (B) is copied to the BM phase panel (A, lower) for comparison. E. Phase differences. Guinea pig 68.

The final data set (Fig. 12) is from the RW region of the cochlea in guinea pig, with BF ~ 45 kHz. These are early data from this approach and due to weak reflectivity and non-pristine condition of this very basal location, we could only detect motion down to 60 dB SPL. The approach had significant transverse and radial components to the optical axis, as is evident in the slanted BM in the B-scan of Fig. 12D. The Fig. 12 results showed similarities to the transversely measured gerbil data of Figs. 4-6, and guinea pig data of Fig. 11: the OHC\DC region contained sub-BF nonlinearity and an amplitude trough at 70 and 80 dB SPL. The OHC\DC-region phase lagged the BM phase in the sub-BF region (E) although by a smaller amount than in the transverse data sets of Figs. 4-6 and Fig. 11. On the high frequency side of the trough, the OHC\DC-region phase joined the BM phase (direct comparison in pink dotted curve), as in Figs. 4-6 and Fig. 11. The RL, BM phase difference was close to zero.

Discussion:

A. OHC-region behavior when optical axis is transverse -- complex differences to find internal motion

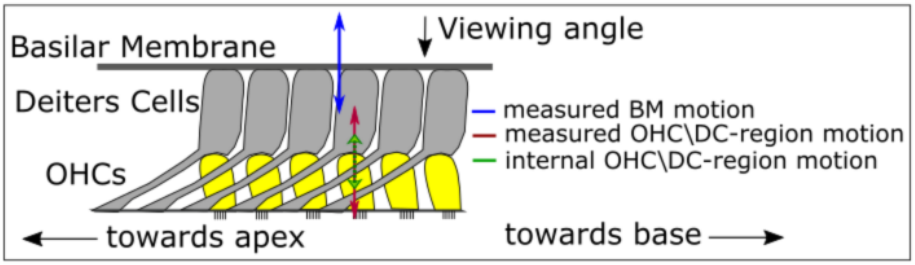

Figure 13. Longitudinal-transverse cartoon of the OCC from the BM to the RL. Diagram of complex difference to find internal OHC-region motion.

The OHC\DC-region measurements made along a transverse optical axis (Figs. 4-6, 11) possessed magnitude troughs and associated phase shifts. These characteristics suggest that the measured OHC\DC-region motion can be considered as a sum of an internal OHC motion and motion of the structure supporting the OHC\DCs. The BM is the primary structural element of the OCC frame and is taken as the support structure. Based on its anatomy, with its set of tightly packed and radially-oriented collagen fibers (de Sousa Lobo Querido et al., 2023; Dreiling et al., 2002), the BM is expected to move primarily in the transverse direction, and this was supported by the BM results in Figs. 7 and 8. Taking the complex difference, OHC\DC-region minus BM motion, produces the internal motion of the OHC\DC-region. This analysis was done for the data of Figs. 4, 6 and 11.

In the analysis of Fig. 14, BM motion is blue, OHC\DC-region motion is maroon and their complex difference is green. Because the BM and OHC\DC-region motions can be nearly out of phase, the magnitude of their difference was often larger than the magnitudes of the OHC\DC region and BM motion -- in particular, the green curves in Fig. 14A at 50-70 dB, in Fig. 14B at 60 dB SPL and Fig. 14C at 50 dB SPL. The magnitude trough is either not present or reduced in the calculated internal motion, and the phase shift observed in the measured motion is no longer present in the internal motion. In Fig. 14A-C, 80 dB SPL curves, the reason for the trough in measured OHC\DC-region motion (maroon) is easily traced to the equal amplitudes and half cycle phase differences of the blue and green curves of BM and internal OHC\DC-region motion. Thus, the results of the complex differencing clarified oddities of the measured motion.

The guinea pig data recording through the RW (Fig. 12) had a substantial radial component and was not included in the vector difference analysis, but the results from Fig. 12 and Fig. 14 suggest that the OHC amplitude trough and phase shift observed in Fig.12 were based in a cancellation between OHC\DC-region and BM motion, akin to the measurements of Figs. 4, 6 and 11. For the data sets taken with a significantly longitudinal optical axis (Figs. 8 - 10), an analysis to reconstruct transverse and longitudinal motion has been devised but requires more extensive data to implement (Frost et al., 2023a,b).

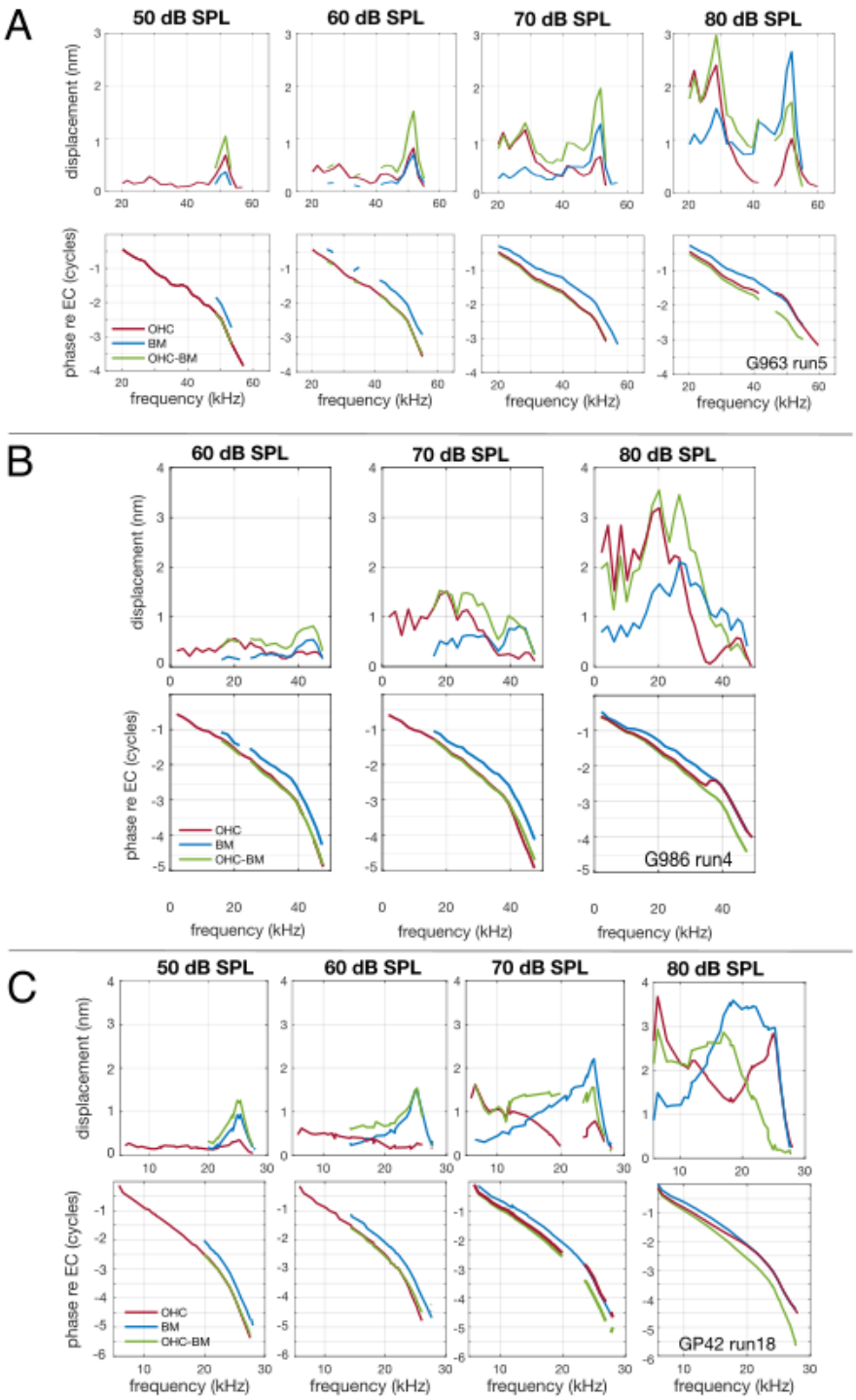

Figure 14. Complex difference between OHC\DC region and BM responses was taken to reveal internal OHC\DC motion. In each preparation the responses going into the difference were measured along a single A-scan as in the motion data of Fig.4 (Gerbil 986), Fig.6 (Gerbil 963), Fig.11 (Guinea Pig 42). Results are shown in panel sets A,B,C, respectively. Each panel set has subpanels corresponding to different SPL and within each subpanel, the OHC and BM data are shown in maroon and blue respectively, and the OHC-BM complex difference is shown in green.

B. Comparison with previous data

The gerbil measurements of Figs. 8 - 10 were made with an approach through the RW opening and angling longitudinally to reach the ~ 25 kHz location. This approach was used in several of our

previous studies and the results presented here are similar to those and the earlier results of Cooper et al., (2018), who also used multitone stimuli. Because of the steep longitudinal angle, the RL is often not observable in this approach, and in our previous reports we emphasized OHC\DC and BM regions.

The gerbil measurements of Figs. 4-6 were made with a nearly transverse approach through the RW. This approach affords a transverse-radial view in the B-scan, and the RL region can be identified. This approach is like that of Cho and Puria, 2022, and the findings were similar. Cho and Puria used single-tone stimuli and in their case the presence of sub-BF activity in the OHC\DC region was observed via *post-mortem* reduction in sub-BF motion. In the RL and BM, sub-BF motion was not reduced post-mortem and the Cho and Puria data support the statement that the RL is within the OCC frame.

The Fig. 7 observations were made through a cochleostomy, to make transverse measurements in the ~ 25 kHz location. The view was limited to the medial OCC and did not include the OHC region. Measurements were made at the BM and 65 μm deeper within the OCC, likely at the RL above the pillar cells. Sub-BF responses were linear; all positions were within the frame. He et al., 2022 made measurements at this BF location through a cochleostomy after surgically displacing the stapedial artery to afford a more complete view of the OCC. Their system did not include B-scan imaging, and they used single-tone stimuli. The region they identified as the RL exhibited a *post-mortem* reduction in motion at all frequencies, including sub-BF, so displayed sub-BF activity. Their finding of sub-BF RL conflicts with our statement that the RL is part of the OCC frame. This difference bears further study.

The relatively large degree of sub-BF nonlinearity in the guinea pig results of Fig. 11 was not noted in our previous report, in which sub-BF nonlinearity was small, and absent in regions that anatomically were within the OHC\DC region (Fallah et al., 2021). The previous findings, coupled with those here, advance a hypothesis that in guinea pig the frame motion dominates the internal non-frame motion over more of the OCC relative to gerbil. The guinea pig data in Fig. 11 and the previous report were gathered with a nearly transverse optical axis. If a more longitudinal optical axis were achievable, which would be sensitive to longitudinal motion and also span through several rows of OHCs, sub-BF nonlinearity might be more prevalent (Cooper et al., 2018). Chen et al., 2011 measured RL and BM motion through a cochleostomy in guinea pig at a similar BF location. They found RL and BM motion to be tuned and nonlinear at BF peak frequencies. Sub-BF the responses in both regions scaled approximately linearly. The stimuli were single tone. Ramamoorthy et al., 2013 made measurements through the RW in guinea pig. They showed one motion data set from within the OCC. The responses were tuned and nonlinear at BF peak frequencies and linear sub-BF. The stimuli were single tone.

C. Significance of frame for hair cell excitation.

In the base of the cochlea, neural tuning is similar to BM motion, especially in the BF peak (Naryanan et al., 1998). Hair cells are stimulated by the pivoting motion of their stereocilia, which in Fig. 2A stand below the RL and insert (OHCs) or nearly insert (IHCs) into the tectorial membrane (Lim, 1972). In the results of this study, the RL appeared to be part of the frame, lacking sub-BF nonlinearity. Thus, it seems that hair cell stereocilia, both IHC and OHC, are not stimulated by the relatively large and nonlinear sub-BF motion that is present in the OHC\DC region. The sub-BF nonlinearity observed in local cochlear microphonic (Fallah et al., 2019) would in that case be due solely to MET nonlinearity, and not to nonlinear input to the OHCs**.** In damaged cochleae high-frequency auditory neurons can become hyper-sensitive to sub-BF tones, and contain temporal firing patterns including phase locking that are not present in healthy high-frequency auditory neurons (Versnel et al., 1996; Kale and Heinz 2010). It is possible that in damaged cochleae the frame can become compromised, allowing OHC activity to overstimulate stereocilia at sub-BF frequencies, leading to pathological auditory nerve responses.

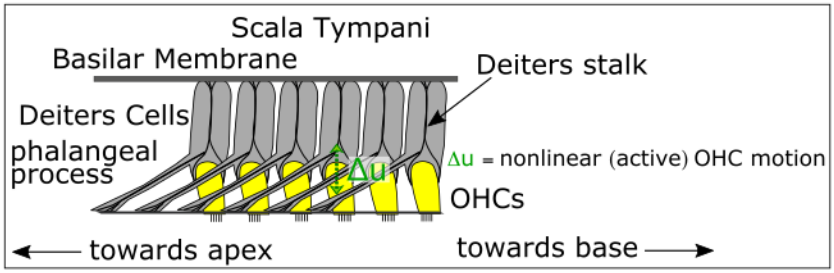

Figure 15. Longitudinal-transverse cartoon of the OCC from the BM to the RL. The nonlinear motion of the OHCs will produce nonlinear forces on the Deiters cells that will be transmitted to the BM and RL.

D. Physical ramifications of OCC frame

Nonlinear motion abutting tissue exerts nonlinear forces. In Fig. 15, Δu is nonlinear OHC motion, compressing and stretching the Deiters cells, which will transmit these forces to the BM and RL. However, sub-BF nonlinear motion is not observed in the BM or RL or other components of the OCC frame. Thus, sub-BF forces on the frame must be dominated by passive forces. A primary force on the BM is the pressure on its scala tympani surface. This pressure is tuned and non-linear in the BF peak but is linear and passive (unchanging *post-mortem*) sub-BF (Olson, 2001). Pressure and BM motion are partners in the cochlear traveling wave, and previous reports have noted that sub-BF activity is not transported by the wave (Fallah et al., 2019; Dewey et al., 2018, Guinan, 2020). The pillar cells and the Deiters stalk, composed of microtubules, actin and intermediate filaments, anchor the RL to the BM (Engstrom and Wersall, 1958; Parsa et al., 2012; Zhou et al., 2022). The physical properties and orientation of these structures work to make the RL move more like the BM, and not like the OHCs. The phalangeal processes of the DCs course apically (Fig. 15) and as the cochlear traveling wave travels apically, their mechanical effect on the RL will be to impose basal BM motion on the more apical location, and thus a phase lead would be imposed. Thus, in transverse measurements of the RL and BM, the RL would be predicted to lead the BM. The value of the predicted phase lead depends on the traveling wave wavelength, which is ~ 0.4 mm at frequencies getting close to the BF (Ren 2002) and longer at lower frequencies. The phalangeal processes in the gerbil base span a longitudinal distance of ~ .08 mm (Wang et al., 2016). Thus, at frequencies approaching the BF the phalangeal processes span ~ 0.2 wavelengths, corresponding to 0.2 cycle. This is close to the measured RL re BM phase lead in Figs. 4F and 6F.

A central mystery of cochlear mechanics remains: how does the BM (and OCC frame in general) respond to OHC forces only at frequencies in the BF peak, where these forces amplify its motion by factors approaching 1000? Mathematical models can replicate this phenomenon (Nankali et al., 2020; Yoon et al., 2011, deBoer and Nuttall, 2000; Altoe et al., 2022; Sisto et al., 2021) but their physiological underpinnings remain tenuous. OCT has delivered a wealth of new data regarding the coordinated responses of OHCs, supporting cells and their surrounding fluid and extracellular structures. In the current analysis, OCT observations have advanced the concept of separate "non-frame" and "frame" motions, whose separation is likely essential for healthy cochlear function.

References

Altoe A, Dewey JB, Charaziak KK, Oghalai JS & Shera CA (2022) Overturning the mechanisms of cochlear amplification via area deformations of the organ of Corti. J Acoust Soc Am 152: 2227-2239.

Chen F, Zha D, Fridberger A, Zheng J, Choudhury N, Jacques SL, Wang RK, Shi X & Nuttall A L (2011) A differentially amplified motion in the ear for near-threshold sound detection. Nature neuroscience 14: 770-774.
Cho NH & Puria S (2022) Cochlear motion across the reticular lamina implies that it is not a stiff plate. Sci Rep 12: 18715.
Cooper NP Vavakou A & van der Heijden M (2018) Vibration hotspots reveal longitudinal funneling of sound-evoked motion in the mammalian cochlea Nature communications 9(1) 1-12
De Boer E & Nuttall AL (2000) The mechanical waveform of the basilar membrane III Intensity effects. J Acoust Soc Am 107:1497-1507.
de Sousa Lobo Querido R, Ji X, Lakha R, Goodyear RJ, Richardson GP, Vizcarra CL & Olson ES (2023) Visualizing collagen fibrils in the cochlea's tectorial and basilar membranes using a fluorescently labeled collagen-binding protein fragment. JARO 24: 1-17.
Dewey JB, Applegate BE & Oghalai JS (2019) Amplification and suppression of traveling waves along the mouse organ of corti: evidence for spatial variation in the longitudinal coupling of outer hair cell-generated forces. J Neurosci 39: 1805–1816.
Dong W & Olson ES (2013) Detection of cochlear amplification and its activation. *Biophysical J* 105: 1067-1078.
Dong W & Olson ES (2016) Two-tone suppression of simultaneous electrical and mechanical responses in the cochlea. *Biophysical J* 111: 1805-1815.
Dreiling FJ, Henson MM & Henson OW Jr (2002) The presence and arrangement of type II collagen in the basilar membrane. Hearing Research 166:166-180.
Engstrom H & Wersall J (1958) The ultrastructural organization of the organ of Corti and of the vestibular sensory epithelia. Experimental Cell Research 14:460-492.
Fallah E, Strimbu CE & Olson ES (2019) Nonlinearity and amplification in cochlear responses to single and multi-tone stimuli. Hearing Research 377:271-281.
Fallah E, Strimbu CE & Olson ES (2021) Nonlinearity of intracochlear motion and local cochlear microphonic: Comparison between guinea pig and gerbil. Hearing Research 405: 108234.
Fettiplace R & Kim KX (2014) The physiology of mechanoelectrical transduction channels in hearing. Physiological Reviews 94: 951-986.
Frank G, Hemmert W & Gummer AW (1999) Limiting dynamics of high-frequency electromechanical transduction of outer hair cells. PNAS 96: 4420-4425.
Frost BL, Strimbu CE & Olson ES (2022) Using volumetric optical coherence tomography to achieve spatially resolved organ of Corti vibration measurements. J Acoust Soc Am 151: 1115-1124.
Frost BL, Strimbu CE & Olson ES (2023a) Reconstruction of transverse-longitudinal vibrations in the organ of Corti complex via optical coherence tomography. J Acoust Soc Am 153: 1347-1360.
Frost BL, Strimbu CE & Olson ES (2023b) Erratum: Reconstruction of transverse-longitudinal vibrations in the organ of Corti complex via optical coherence tomography [J Acoust Soc Am 153 1347-1360]. J Acoust Soc Am 153: 2537.
Guinan JJ Jr. (2022) Cochlear amplification in the short-wave region by outer hair cells changing organ-of-Corti area to amplify the fluid traveling wave. Hearing Research 426: 108641.
He W, Burwood G, Porsov EV, Fridberger A, Nuttall AL & Ren T (2022) The reticular lamina and basilar membrane vibrations in the transverse direction in the basal turn of the living gerbil cochlea. Sci Rep 12: 19810.
Iwasa KH & Adachi M (1997) Force generation in the outer hair cell of the cochlea. Biophysical J 73: 546-555.

Kale S & Heinz MG (2010) Envelope coding in auditory nerve fibers following noise-induced hearing loss. JARO 11: 657-673.
Nankali A, Wang Y, Strimbu CE, Olson ES & Grosh K (2020) A role for tectorial membrane mechanics in activating the cochlear amplifier. Sci Rep 10: 17620.

Narayan SS, Temchin AN, Recio A & Ruggero MA (1998) Frequency tuning of basilar membrane and auditory nerve fibers in the same cochleae. Science 28: 1882-1884.
Olson E S (2001) Intracochlear pressure measurements related to cochlear frequency tuning J Acoust Soc Am 110(1) 349-367.
Parsa A, Webster P & Kalinec F (2012) Deiters cells tread a narrow path: The Deiters cells-basilar membrane junction. Hearing Research 290: 13-20.
Ramamoorthy S, Zhang Y, Petrie T, Chen F, Subhash HM, Choudhury N, Wang R, Jacques SL & Nuttall AL (2013) Measurement of in vivo basal-turn vibrations of the organ of Corti using phase-sensitive Fourier domain optical coherence tomography. Proceedings of SPIE 8565: 85651.
Rhode WS (2007) Basilar membrane mechanics in the 6–9 kHz region of sensitive chinchilla cochleae. J Acoust Soc Am 121:2792-2804.
Sisto R, Belardinelli D & Moleti A (2021) Fluid focusing and viscosity allow high gain and stability of the cochlear response. J Acoust Soc Am 150: 4283-4296.
Strimbu CE Wang Y & Olson ES (2020) Manipulation of the endocochlear potential reveals two distinct types of cochlear nonlinearity Biophysical J 119: 1-15.
van der Heijden M & Joris PX (2003) Cochlear phase and amplitude retrieved from the auditory nerve at arbitrary frequencies. J Neurosci 23(27) 9194-9198.
Strimbu CE & Olson E S (2022) Salicylate-induced changes in organ of Corti vibrations. Hearing Research 423: 108389.
van der Heijden M & Joris PX (2003) Cochlear phase and amplitude retrieved from the auditory nerve at arbitrary frequencies. J Neurosci 23:9194–9198.
Versnel H, Prijs VF & Schoonhoven R (1997) Auditory-nerve fiber responses to clicks in guinea pigs with a damaged cochlea J Acoust Soc Am 101: 993-1009.
Versteegh CP & van der Heijden M (2012) Basilar membrane responses to tones and tone complexes: nonlinear effects of stimulus intensity. JARO 13: 785-798.
Wang Y, Steele CR & Puria S (2016) Cochlear outer-hair-cell power generation and viscous fluid loss. Sci Rep 6:19475.
Warren RL, Ramamoorthy S, Ciganovic N & Lim DJ (1972) Fine morphology of the tectorial membrane: its relationship to the organ of Corti. Arch Otolaryngology 96:199–215.
Yoon YJ, Steele CR & Puria S (2011) Feed-forward and feed-backward amplification model from cochlear cytoarchitecture: an interspecies comparison. Biophysical J 100: 1-10.
Zhou W, Jabeen T, Sabha S, Becker J & Nam J-H (2022) Deiters cells act as mechanical equalizers for outer hair cells J Neurosci 42:8361-8372.